Chaotic tip trajectories of a single spiral wave in the presence of heterogeneities

Daniel M. Lombardo and Wouter-Jan Rappel*
Department of Physics, University of California San Diego, San Diego, California 92093, USA

(Received 7 December 2017; revised manuscript received 8 February 2019; published 17 June 2019)

Spiral waves have been observed in a variety of physical, chemical, and biological systems. They play a major role in cardiac arrhythmias, including fibrillation, where the observed irregular activation patterns are generally thought to arise from the continuous breakup of multiple unstable spiral waves. Using spatially extended simulations of different electrophysiological models of cardiac tissue, we show that a single spiral wave in the presence of heterogeneities can display chaotic tip trajectories, consistent with fibrillation. We also show that the simulated spiral tip dynamics, including chaotic trajectories, can be captured by a simple particle model which only describes the dynamics of the spiral tip. This shows that spiral wave breakup, or interactions with other waves, are not necessary to initiate chaos in spiral waves.

DOI: 10.1103/PhysRevE.99.062409

I. INTRODUCTION

Spiral waves are generic dynamical states of spatially extended excitable systems. They are observed in a variety of biological and nonbiological systems, including aggregates of Dictyostelium discoideum cells [1], chicken retinas [2], surface catalytic oxidation reaction systems [3], and in chemical Belousov-Zhabotinsky systems [4,5]. Spiral waves can also form in cardiac tissue, where they are believed to play a critical role in life-threatening arrhythmias [6]. In particular, they are responsible for the maintenance of fibrillation during which the activation pattern of the tissue is incoherent, resulting in insufficient pumping of blood [7–11].

Spiral waves are characterized by a tip, corresponding to a phase singularity, and a rotating wave that propagates outwards. Simulations have revealed that the tip trajectory of a single, stable spiral wave can trace a variety of periodic patterns [12–17]. These patterns include circular trajectories, regular meandering trajectories, and hypermeandering trajectories, during which the tip traces an irregular path. Many computational studies have also demonstrated that spiral waves can be unstable, both in homogeneous and in highly heterogeneous domains [6,18–21]. This instability leads to continuous breakup and formation of new spiral waves, accompanied by removal of spiral waves through collisions. This multiwave state results in incoherent activity, consistent with recordings of fibrillation.

Recent studies in humans have demonstrated the existence of spatially localized spiral sources during atrial fibrillation [9–11,22]. The ablation of tissue at these locations can result in acute termination of fibrillation, suggesting that these localized spirals are the driving factor of fibrillation [23]. Furthermore, it suggests that these tissue regions have different electrophysiological properties, consistent with the observation that cardiac tissue is rarely homogeneous and typically exhibits variations either due to inherent differences in cell properties [24] or due to injury and disease such as ischemic fibrosis [25]. In these studies, fibrillation would not require a multispiral state but, instead, can be due to a single spiral wave. Consistent with this hypothesis is that tracking of the spiral tip of the localized source has revealed that it does not appear to trace a regular path, but instead displays a complex trajectory [10,26]. Thus, the question arises: Can a single spiral in the presence of a small number of heterogeneities exhibit irregular tip trajectories, and can it generate irregular activations patterns even in the absence of spiral wave breakup?

We address this question by computationally examining the trajectory of a single spiral wave in the presence of tissue heterogeneities, modeled as small regions with decreased excitability. Previous numerical studies have shown that a spiral wave can be attracted to an isolated heterogeneity, causing it to eventually be anchored and resulting in a regular activation pattern [19,27–31]. Furthermore, a recent study has shown that multiple heterogeneities can have a profound impact on the stability of spiral waves and can result in chaotic activation patterns consisting of multiple spiral waves [32]. Here, we will show that the tip trajectory of a single spiral can become chaotic in the presence of just two small heterogeneities and that these dynamics can be captured by a simple model in which the tip is represented by a particle in a force field.

II. TIP DYNAMICS OF ELECTROPHYSIOLOGICAL MODELS

We start with a standard model for cardiac tissue which describes the potential u of cardiac cells as

$$\frac{du}{dt} = D\nabla^2 u - \frac{I_{\text{ion}}}{C_m}. \tag{1}$$

Here D is a diffusion coefficient responsible for the spreading of the activation front and C_m is the capacitance of the membrane. I_{ion} represents the membrane currents and models for these currents range from relatively simple to very detailed

*Address for correspondence: Wouter-Jan Rappel, PhD, University of California, San Diego CA 92093; rappel@physics.ucsd.edu

TABLE I. Parameters used for the Fenton Karma model simulations as shown in the main text. All time constants τ are in milliseconds, all voltages are in rescaled, arbitrary units. The diffusion constant has units of cm^2/ms.

Parameter	Set I	Set II
τ_v^+	3.33	3.33
τ_{v1}^-	19.6	19.6
τ_{v2}^-	1000	1000
τ_w^+	50	50
τ_w^-	11	11
τ_d	0.43	0.403
τ_o	8.3	8.3
τ_r	50	50
τ_{si}	45	45
k	10	10
V_c^{si}	0.85	0.85
V_c	0.13	0.13
V_v	0.055	0.055
D	0.001	0.001

[33]. We used both a simplified electrophysiological model, the Fenton-Karma (FK) model [34] which contains only 3 currents and 13 parameters, and the detailed Koivumäki, Korhonen, and Tavi (KKT) model, which contains 13 currents and more than 40 parameters [35]. The parameters of the FK model can easily be changed to fit different electrophysiological data, including human [18,36], while the KKT model has been specifically developed for human atrial tissue [37–39].

The equations for the gating variables (v, w) and the currents (I_{fi}, I_{so}, I_{si}) for the FK model used in our study are:

$$\frac{dv}{dt} = \frac{[1-H(u-V_c)](1-v)}{[1-H(u-V_v)]\tau_{v1}^- + H(u-V_v)\tau_{v2}^-} - \frac{H(u-V_c)v}{\tau_v^+}. \tag{2}$$

$$\frac{dw}{dt} = \frac{[1-H(u-V_c)](1-w)}{\tau_w^-} - \frac{H(u-V_c)w}{\tau_w^+} \tag{3}$$

$$I_{fi} = -\frac{H(u-V_c)(u-V_c)(1-u)v}{\tau_d} \tag{4}$$

$$I_{so} = \frac{u[1-(u-V_c)]}{\tau_o} + \frac{H(u-V_c)}{\tau_r} \tag{5}$$

$$I_{si} = -w\frac{1+\tanh\left[k\left(u_i - V_c^{si}\right)\right]}{2\tau_{si}} \tag{6}$$

where H is the heaviside step function and u is the membrane potential. We used two parameter sets, set I and set II, for the FK model which are listed in Table I. The equations of the KKT model are to numerous to reproduce here and can be found in the literature [35,37]. Parameters for the KKT model are based on the most recently published values [37] and are given in Table II.

Our simulations were performed on a two-dimensional square sheet with a spatial discretization of 0.025 cm and a side length of 200 elements (FK model) or 400 elements (KKT model) and no-flux boundary conditions. The time step

TABLE II. Parameters used for the KKT model simulations as shown in the main text. PNa was lowered to 0.001 nL/s to improve stability of the spiral wave.

Parameter	Value
Na_o(mM)	130.0
Ca_o(mM)	18.0
K_o(mM)	5.4
C_m(nF)	0.05
B_{Na}(mM)	1.132
Kd_{BNa}(mM)	10.0
I_{NaKmax}(pA)	70.0
k_{NaKK}(mmol/L)	1.0
k_{NaKNa}(mmol/L)	11.0
B_{Ca}(mM)	0.024
Kd_{BCa}(mM)	2.38E-03
P_{Na}(nL/s)	1.0E-03
$E_{Ca_{app}}$(mV)	60
kCa_n	2
k_{Ca}(mM)	6.00E-04
I_{CaPmax}(pA)	2
k_{CaP}(mM)	5.00E-04
γ	0.45
d_{NaCa}(mmol/L)$^{-4}$	3.00E-04
D_{Ca}($\mu m^2/s$)	780
D_{CaSR}($\mu m^2/s$)	44
D_{CaBm}($\mu m^2/s$)	25
D_{Na}($\mu m^2/s$)	0.12
k_4(s^{-1})	13
k_{SRleak}(s^{-1})	6.00E-03
CSQN(mM)	6.7
Kd_{CSQN}(mM)	0.8
k_{NaCa}(pA/(mmol/L)^4)	0.0084
g_{Ks}(nS)	1
g_{K1}(nS)	3.45
g_{Nab}(nS)	0.0606
g_{Cab}(nS)	0.0952
g_{If}(nS)	1.0
g_{CaL}(nS)	15.0
g_t(nS)	8.25
g_{sus}(nS)	2.25
g_{Kr}(nS)	0.50
SLlow(mM)	165.0
SLhigh(mM)	13.0
Kd_{SLlow}(mM)	1.10
Kd_{SLhigh}(mM)	13E-3
D(cm^2/ms)	1.00E-03

was chosen to be 0.05 and 0.01 ms for the FK and KKT model, respectively. We used the Cuda parallel computing platform to calculate each grid element simultaneously, resulting in very efficient computational algorithms. Numerical integration was performed using the forward Euler method, and we simulated a 60-s time segment. In order to allow the system to reach a steady state, only the last 30 s of the simulation were recorded. The coordinates of the tip trajectory were saved every 5 ms. We have verified that the results did not significantly change if the time step was lowered by a factor of 5.

We first focused on the FK model, which can produce a variety of stable, regular single spiral trajectories in homoge-

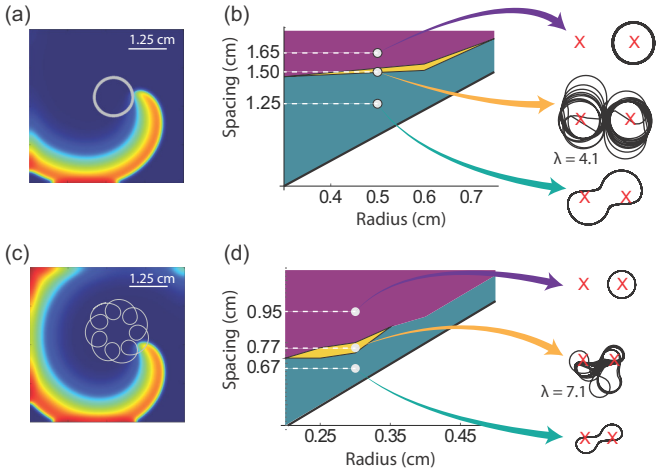

FIG. 1. (a), (c) Snapshot of a counterclockwise rotating spiral wave for two different parameter sets of the FK model [voltage color-coded ranging from high (red) to low (blue) values, tip trajectory shown in white; (a) set I, (c) set II]. (b), (d) Phase diagrams in the spacing-size space for the FK model. In this, and all other figures, blue area indicates regular trajectories that wrap around both heterogeneities, purple region represents tip trajectories that circle either one of the heterogeneities, and yellow region corresponds to chaotic trajectories. Displayed spiral tip trajectories correspond to the white dots in the phase diagram. Red X's mark the locations of the circular regions with decreased excitability. Lyapunov exponents (λ) for the chaotic trajectories are given in units of bits/second [(b) set I, (d) set II].

neous media by varying just a few of the parameters [18]. This is evident from Figs. 1(a) and 1(c) where we show snapshots of a simulation using parameter set I (A) and II (C). The power spectrum of the time series of the x coordinate of the tip for set I shows a single peak while for set II it shows two peaks [Fig. 2(a)]. Furthermore, set I produces a circular trajectory and set II results in a flowerlike trajectory with inward petals, shown in more detail in Fig. 2(b).

To examine how the model behaves in heterogeneous media, we added two identical, circular regions with decreased excitability to the computational domain. Within these regions we decreased the excitability of the fast inward current by raising the value of the parameter τ_d to 0.5 ms. For consistency, the initial conditions used in each simulation consisted of a spiral wave in the lower left region of the sheet. We adjusted the size and spacing between the heterogeneities, and quantified their effects on the dynamics of the spiral wave trajectory. We have verified that these effects are relatively insensitive to initial conditions and that, as long as the spiral wave trajectory crosses the heterogeneity at some point in time, the resulting dynamics will be similar to what is reported here.

Our simulations revealed that the presence of the two circular heterogeneities can dramatically alter the tip trajectory of the spiral wave and the activation patterns of the tissue. This is shown in Figs. 1(b) and 1(d), where we have plotted phase diagrams of the tip trajectory found in the simulations corresponding to sets I and II. In these diagrams the x axis represents the heterogeneity size while the y-axis represents the spacing between heterogeneities. Since very small heterogeneities leave the trajectory unaffected, we only focus on heterogeneity sizes that are large enough to alter the tip behavior. Also, note that since the distance between the heterogeneities is at least twice their radius, the phase diagram is only shown above the line $y = 2x$. The phase diagram shows that for small spacings, the spiral wave is anchored to both heterogeneities and orbits around them [blue region, Figs. 1(b) and 1(d)], while for large spacings the spiral wave rotates around one of the two heterogeneities [purple region, Figs. 1(b) and 1(d)]. The regular, periodic spiral tip trajectories corresponding to a representative point within these two regions are also shown in Figs. 1(b) and 1(d). Interestingly, there is a region in phase space between these two regular domains for which the trajectory becomes irregular. Within this region, the spiral tip alternately circulates, in a nonperiodic fashion, around one or the other heterogeneity. Thus, the presence of a pair of heterogeneities is sufficient to drastically alter the tip dynamics of a single spiral and to render it irregular. To ensure this behavior is not caused by the boundary conditions, we have confirmed that doubling the domain size produces similar results. We further verified that the spiral wave does not breakup into multiple waves, and remains a single spiral throughout the simulation.

To quantify the dynamics of the irregular trajectories, we computed the leading Lyapunov exponent, λ, which measures the rate of exponential divergence of nearby trajectories using a standard procedure [40] (see Appendix A). We found that λ for the irregular patterns, corresponding to the yellow region in the phase diagrams of Figs. 1(b) and 1(d), was large and

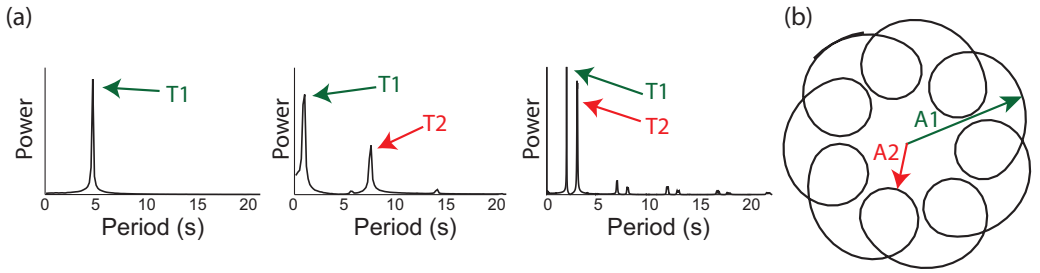

FIG. 2. (A) Power spectrum of the x component of the tip trajectory for the different electrophysiological models and parameter sets used in the main text. The spectra have either one or two peaks, corresponding to the frequencies $\omega_1 = 2\pi/T_1$ and $\omega_2 = 2\pi/T_2$ (left panel, FK set I; middle panel, FK set II; right panel, KKT). (B) The spiral tip trajectory for set II. The maximum and minimum value of the spatial extent of the tip trajectory are denoted by A_1 and A_2, respectively.

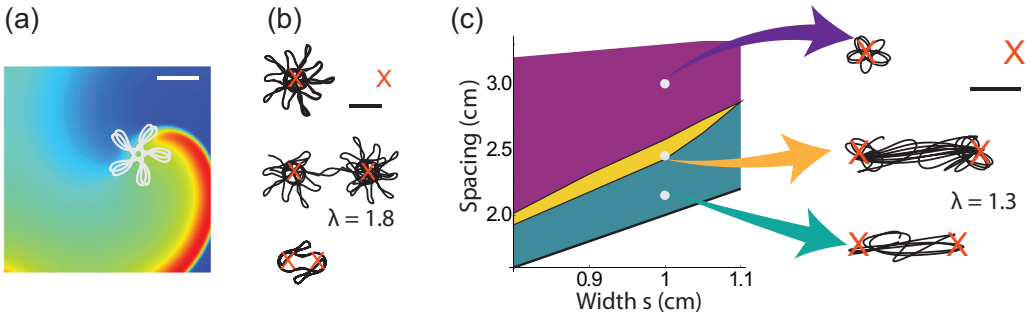

FIG. 3. (A) Snapshot of a counterclockwise rotating spiral wave in the homogeneous KKT model. (B) Sample tip trajectories of the KKT model, for different spacings of heterogeneities with radius 0.5 cm. (C) Phase diagrams of tip trajectories for the SP model. All scale bars are 1 cm. See also Fig. 1.

positive, while for the regular tip trajectories it was close to zero. Therefore, our simulations show that the presence of heterogeneities and a single spiral wave are sufficient to produce chaotic dynamics.

We then investigated the KKT model [35,37], which, in homogeneous tissue, exhibits a spiral wave that is stable, with a tip trajectory that shows a flower pattern with outward petals [Fig. 3(a)]. The power spectrum of the tip coordinates again shows only two dominant frequencies [Fig. 2(a)]. We then added circular heterogeneities by decreasing the permittivity of the sodium channel I_{Na} to half of its original value. Since this model is computationally much more demanding than the FK model, we did not map out the entire phase space shown in Fig. 1. Instead, we fixed the radius of the heterogeneities to 0.5 cm and varied their spacing, corresponding to a cut through phase space. The results are shown in Fig. 3(b), where we have plotted the tip trajectory for different spacings of the heterogeneities. As in the case of the FK model, the KKT model shows regular dynamics when the spacing is small, with a tip trajectory that spans both heterogeneities, and when the spacing is large, corresponding to the tip rotating around one of the heterogeneities. For intermediate spacings, the trajectory alternates in a nonregular fashion between the two heterogeneities and computing the Lyapunov exponent revealed that the dynamics was chaotic. Thus, as found in the FK model, a single spiral wave in the presence of heterogeneities can produce chaotic activation patterns.

III. DYNAMICS OF A SINGLE PARTICLE MODEL

Previous studies have noted that spiral waves in excitable media exhibit both wavelike and particlelike properties [41,42]. The waves can react to small perturbations as particlelike objects and asymptotic theories have been developed to describe their interactions with periodic perturbations and localized inhomogeneities [43,44]. Furthermore, previous studies have described the dynamics of spiral tips in terms of ordinary differential equations near bifurcation points [45,46] and have developed simple equations for circular tip trajectories in the presence of periodic modulations [47].

Here, we constructed a simple model in which the tip trajectory is described by a single particle moving in a potential landscape and subject to periodic forcing terms. The aim is to describe the transition between regular and chaotic trajectories shown in our spatially extended simulation. Our single particle (SP) model is a phenomenological description of the tip trajectory and consists of equations for the x and y coordinates of the tip in the presence of external forces. Contrary to these earlier studies, the model includes an explicit description of heterogeneities. To reproduce the tip trajectories in homogeneous tissue we include two forcing terms with frequencies ω_1 and ω_2 and amplitudes F_1 and F_2, respectively. We note that, if necessary, it is trivial to extend the equations to include forcing terms with more frequencies. Our equations take the form

$$\frac{d^2x(t)}{dt^2} = F_1\cos(\omega_1 t+\phi) + F_2\cos(\omega_2 t) - \xi\frac{dx}{dt} - \frac{dU(x,y)}{dx}, \tag{7}$$

$$\frac{d^2y(t)}{dt^2} = F_1\sin(\omega_1 t) + F_2\sin(\omega_2 t) - \xi\frac{dy}{dt} - \frac{dU(x,y)}{dy}, \tag{8}$$

where the phase ϕ determines whether the pattern is inward ($\phi = 0$) or outward ($\phi = \pi$) and where the third term represents a damping that prevents the model from drifting and allows it to converge to a steady state quickly. The last term in the model describes a potential energy landscape that can be added to model heterogeneities and which is described below.

For the case of homogeneous media [$U(x,y) = 0$] the model can be trivially solved and the parameters can be immediately determined from the tip trajectory computed using the spatially extended electrophysiological models. First, the frequencies ω_1 and ω_2 are simply the frequencies obtained from the power spectrum of the trajectory [Fig. 2(a)]. The value of ω_1 is related to the overall period of the spiral, while ω_2 is the angular frequency of the petals in the flower patterns. Second, the amplitudes of the forcing terms, F_1 and F_2, are determined by the overall size of the trajectory, and the size of the petals [Fig. 2(b)]. Explicit expressions that relate these amplitudes to the maximum, A_1, and minimum value, A_2, of the spatial extent of the tip trajectory are given in Appendix B, along with the complete solution for the homogeneous case. Obviously, for circular tip patterns $\omega_2 = 0$ and $F_2 = 0$ and the model contains only a single forcing term.

Using parameter values obtained as described above we find that the SP model is able to faithfully reproduce the

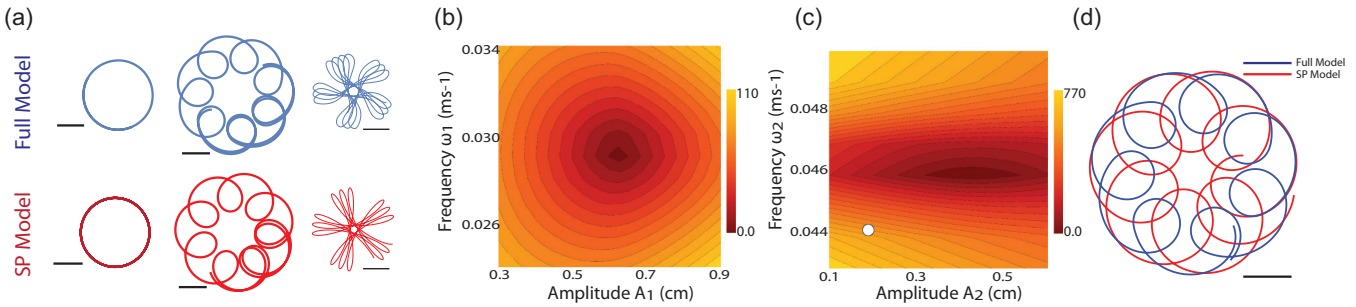

FIG. 4. A: Comparison between the full models (FK set I right panel, FK set II middle panel, and KKT right panel) and SP model for homogeneous media. Scale bars are 0.5 cm. (B, C) Cumulative error (measured in cm, and plotted using a color scheme) in the tip trajectory from the SP model for set I (B) and set II (C) as compared to the trajectory of the full model. The error was computed for every ms and for an entire rotation of the full model. (D) Example of a trajectory of the SP model for the nonoptimal parameters corresponding to the white symbol in C ($A_1 = 1.075$ cm, $A_2 = 0.2$ cm, $\omega_1 = 0.0058\,\mathrm{ms}^{-1}$, and $\omega_2 = 0.0439\,\mathrm{ms}^{-1}$).

tip trajectories for the homogeneous cases. This is shown in Fig. 4(a) where we plot the trajectories for the FK and KKT models (blue) along with the trajectories of the corresponding SP model (red). The parameters of these SP models are listed in Table III. To determine the parameter sensitivity of the SP results we determined the trajectories for a range of parameter values. These trajectories were then quantitatively compared to the trajectory obtained from the full model. For this, we computed the Euclidean distance d between the tip position of the FK model $(x_{\mathrm{FK}}, y_{\mathrm{FK}})$ and of the SP model $(x_{\mathrm{SP}}, y_{\mathrm{SP}})$ for each ms

$$d = \sqrt{(x_{\mathrm{FK}} - x_{\mathrm{SP}})^2 + (y_{\mathrm{FK}} - y_{\mathrm{SP}})^2} \tag{9}$$

The total error was then defined as the sum of d over a full rotation of the FK model (214 ms for set I, and 1080 ms points for set II).

The results of these simulations are shown in Figs. 4(b) and 4(c), where we plot the error for the FK sets I and II models in the A_1-ω_1 and A_2-ω_2 parameter space, respectively, using a color coded scheme. As expected, parameter values obtained using the derived expressions result in trajectories that can most faithfully reproduce the results of the full model. Deviations from these values lead to trajectories with different periodicity and shape. An example of such a less-than-perfect trajectory is shown in Fig. 4(d), corresponding to the parameter values of the white dot in Fig. 3(c). Note that for set I the graph represents the entire parameter space of the SP model. For set II, however, the results are shown for fixed values of A_1 and ω_1 obtained using the explicit expressions in Appendix B and values listed in Table III. We have verified that the results do not change qualitatively when other parameter combinations are kept fixed.

We next investigated the effect of including heterogeneities in the SP model, keeping the forcing parameters fixed to the values determined for the homogeneous case. Circular heterogeneities can be incorporated in the SP model by introducing a potential energy term with circular symmetry and that has a local minimum at the locations of the heterogeneities. Here, we chose a potential of the form

$$U(x,y) = -\frac{g}{\sqrt{2\pi}}\left\{ \exp\left[-\frac{(x-c_{x1})^2 + (y-c_{y1})^2}{2s^2} \right] + \exp\left[-\frac{(x-c_{x2})^2 + (y-c_{y2})^2}{2s^2} \right] \right\}. \tag{10}$$

In this potential, the heterogeneities are described by two Gaussian wells with circular symmetry that are centered at coordinates (c_{x1}, c_{y1}) and (c_{x2}, c_{y2}), respectively (Fig. 5). The width of the Gaussian wells, s, determines the size of the heterogeneous region. The parameter g controls the depth of the wells, and therefore the strength of the heterogeneities. Here we report results for a value of $g = 0.0022\ \mathrm{cm}^2/\mathrm{ms}^2$ to match the dynamics of set I and II, and $g = 0.0088\ \mathrm{cm}^2/\mathrm{ms}^2$ for matching the KKT spiral dynamics. Note that an exact mapping of the effects of heterogeneities in the full model to the potential of the SP model is not possible. Therefore, the trajectories of the tips in the full model will no longer match exactly those of the SP model. The qualitative dynamics, however, can be similar, as we will describe below.

We then determined whether the SP model in the presence of heterogeneities was able to qualitatively reproduce the FK and KKT results. Figures 6(a) and 6(b) show phase diagrams and tip trajectories for the SP model with parameters based on sets I and II of the FK model. For both sets, the phase diagrams are qualitatively similar to the ones obtained using

TABLE III. The parameters for the SP model that reproduce the homogeneous patterns of set I, set II, and the KKT model in the main text. The forcing terms F_1 and F_2 can be found from A_1 and A_2 using the equations given above.

Pattern	ξ (1/ms)	F_1 (cm/ms^2)	F_2 (cm/ms^2)	A_1 (cm)	A_2 (cm)	T_1 (ms)	T_2 (ms)	ϕ
FK (set I)	0.05	0.001	0.0	0.625	0.625	214	—	0
FK (set II)	0.05	2.1E-4	1.1E-3	1.075	0.347	1080	137	0
KKT	0.05	5.4E-4	7.2E-4	1.574	0.1374	518	335	π

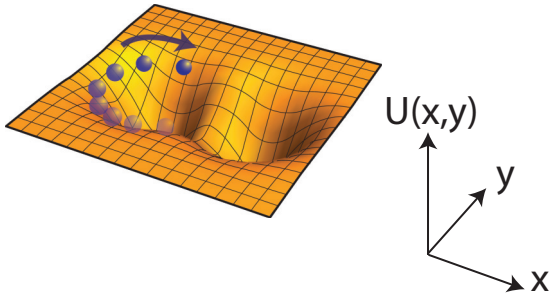

FIG. 5. Schematic representation of a particle moving in a potential landscape with two wells, representing tissue heterogeneities.

the FK model [Figs. 1(b) and 1(d)]. Specifically, for small spacing, the trajectory migrates around both heterogeneities while for large spacing the particle migrates around one of the two heterogeneities. In both cases, the trajectory dynamics is regular with a Lyapunov exponent close to zero. For intermediate spacings, however, there is a region in parameter space for which the spiral tip describes an irregular pattern. In this region, the largest Lyapunov exponent was found to be large and positive, indicating chaotic particle trajectories. In Fig. 3(c) we show the phase diagram results for the SP model with parameters corresponding to the KKT model. Note that contrary to the KKT model, it is computationally trivial to obtain this diagram. The phase diagram shows a similar structure as the phase diagram for the FK model with a chaotic region sandwiched between regular and periodic regions. The trajectories within these regions show good qualitative agreement with the ones obtained using the KKT model. We should point out that anisotropy can also be included into the SP model by modifying the forcing terms for the x and y coordinates, as shown in Appendix B. Since the SP model only describes the tip and not the entire spiral wave, these results show that the tip dynamics does not critically depend on the properties of the spiral wave arms. Furthermore, our results demonstrate that the existence of a chaotic region for a single spiral wave in the presence of heterogeneities is not dependent on the specifics of the model, but rather a generic property of spiral waves.

As for the case without heterogeneities, we addressed the parameter sensitivity of the SP model. In particular, we determined how the depth g affected the trajectories by computing the trajectories for different values of this parameter. The results can be seen in Fig. 6(c) where we plot the phase diagram of trajectories in the spacing-g space for $s = 0.5$ cm. Small values of g correspond to minor conductance variations in the electrophysiological models and lead to less significant effects on the tip trajectory. As a result, the region in which the tip trajectory orbits both heterogeneities increases in size and no chaotic region is present. For large values of g, corresponding to more fully nonconducting regions, trajectories are increasingly trapped by the heterogeneities. Therefore, upon increasing the spacing between the heterogeneities, the trajectory changes abruptly from orbiting around a single heterogeneity to orbiting around both heterogeneities. Thus, the region of chaotic trajectories is only present for intermediate values of g.

Finally, we show that these results are not limited to a pair of heterogeneities by examining the trajectories of the models in the presence of six, equal-sized heterogeneities, randomly assigned to a coarse grid. For some of these configurations, the FK model displays a regular, periodic trajectory, as seen in Fig. 7(a). This same type of trajectory, in which the tip circles around two heterogeneities, is also captured by the SP model, again using model parameters corresponding to the homogeneous case [Fig. 7(b)]. We have verified that this correspondence holds for 9 out of 10 randomly selected configurations. Furthermore, for some configurations the FK model displays a chaotic trajectory, as determined by computing the Lyapunov exponents [Fig. 7(c)]. This chaotic dynamics is also consistent with the dynamics obtained by the SP model for the same configuration, again demonstrating that the simple particle model is able to qualitatively capture the dynamics of the more complex spatially extended model [Fig. 7(d)]. To determine the effect of the chaotic spiral tip trajectory on recordings of electrical activity, we computed the electrocardiogram (ECG) at a location near one of the heterogeneities [48]. As seen in the inset of Fig. 7(c), the ECG is irregular, resembling ECGs seen during cardiac fibrillation. Importantly though, this irregular ECG is not due to spiral wave breakup but is solely due to the presence of a single spiral wave with a chaotic tip trajectory.

IV. SUMMARY

To summarize, we have demonstrated that the presence of a pair of heterogeneities is sufficient to change the tip trajectory of a single spiral from periodic to chaotic, demonstrating

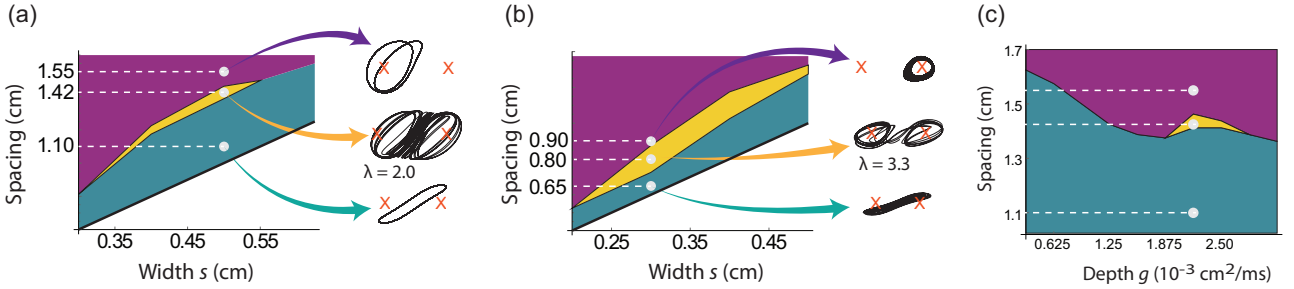

FIG. 6. A, B: Phase diagrams of tip trajectories for set I (A) and set II (B) in the SP model, with tip trajectories and Lyapunov exponents. See also Fig. 1. (C) Phase diagram for set I, illustrating the effect of different well depths g. The circles correspond to the parameter values of the circles in (A).

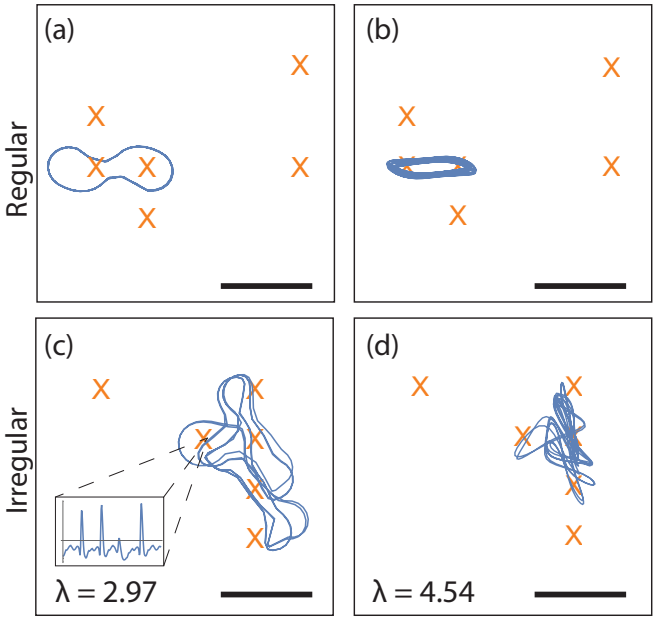

FIG. 7. Spiral trajectories for the FK (left column) and SP models (right column) in the presence of six randomly placed heterogeneities. Regular (A, B) and chaotic (C, D) trajectories with matching placement of the heterogeneities. The radius of the heterogeneities in the FK model was 0.3 cm, and the s parameter in the SP model was 0.275 cm. All scale bars are 1 cm.

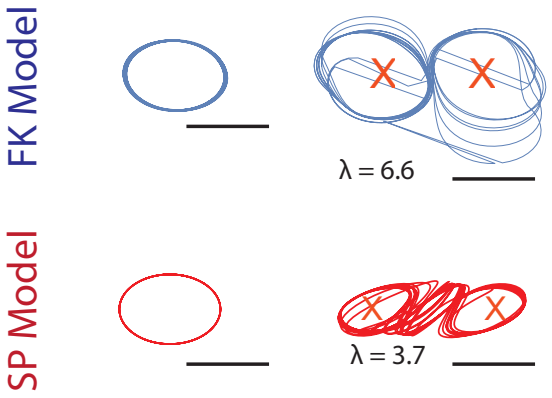

FIG. 8. Example trajectories for the homogeneous (left column) and heterogeneous (right column) case with added anisotropy. In the FK model, the diffusion constant in the y (vertical) direction was chosen to be 50% of the value for the homogeneous case (i.e., $D_y = 0.0005$ cm^2/ms). In the SP model, the forcing amplitude in the x and y equation can be directly determined from the tip trajectory in the homogeneous FK model. The tip trajectories in the SP model capture the FK trajectories for both the homogeneous (left column) and heterogeneous case (right column). Specifically, the chaotic regime is still present in both models. All scale bars are 1 cm.

that spiral wave breakup is not required to generate complex and irregular activity. Note that, similar to the mother rotor hypothesis, this single spiral wave may drive further complex dynamics, including wave break [49]. We have also developed a model of the spiral tip trajectory with parameters that can be directly determined from tip trajectories obtained using spatially extended simulations. This model can accurately capture both the stable spiral tip trajectories observed in spatially extended homogeneous models and can qualitatively capture the transition from periodic to chaotic trajectories observed in heterogeneous models. Our results indicate that this transition is largely independent of the dynamics of the spiral wave arm and the type of electrophysiological model.

ACKNOWLEDGMENTS

We gratefully acknowledge the support of NVIDIA Corporation with the donation of the Tesla K40 GPU used for part of this research. This work was supported by National Institutes of Health R01 Grant No. HL122384.

APPENDIX A: METHOD OF ESTIMATING LYAPUNOV EXPONENTS

As a measure of chaos for each of the spiral trajectories in the two models, the dominant Lyapunov exponent was estimated using a procedure developed by Wolfe *et al.* [40]. This exponent is a measure of how many bits of information are lost per second of simulation time and a positive value of λ indicates that the dynamics is chaotic. We used a publicly available Matlab version of this procedure. First, an attractor is constructed from delay coordinates of the time series of the tip trajectory. The Lyapunov exponent is then approximated by looking at two nearby points in the phase space and observing how the distance between them changes as the system evolves. If the separation grows past a given tolerance, then a new set of points is chosen and the process is repeated. A more detailed description of the method can be found in both the original paper, and the documentation for the Matlab code.

Both four- and three-dimensional delay coordinates were used for calculating the dominant exponent, as recommended in the original paper. It was found that the results did not significantly vary between the two, and so all values are reported with the four-dimensional delay coordinates. The time delay was set to be approximately equal to 1/3 the orbital period, and varies for different configurations. The tolerance level for the distance, determining when to stop the comparison between two points and choose a new set, is set to be between 10–15% of the spatial extent of the x-coordinate of the tip trajectory. For all simulations shown here, the tip position is recorded once every 5 ms, giving approximately 20 to 50 points per orbit. The final output of the Lyapunov exponent is given in units of bits/second. This is then an indication of how many bits of information are lost each second of the simulation.

APPENDIX B: ANALYTIC SOLUTION FOR THE PARTICLE MODEL

For the specific case of homogeneous media, the equations for the SP model become analytically solvable:

$$\begin{aligned} x(t) = &-\frac{e^{-\xi t}}{\xi}C_{1x} + C_{2x} \\ &+ F_1\frac{\xi\sin(\omega_1 t+\phi) - \omega_1\cos(\omega_1 t+\phi)}{\omega_1\left(\xi^2+\omega_1^2\right)} \\ &+ F_2\frac{\xi\sin(\omega_2 t) - \omega_2\cos(\omega_2 t)}{\omega_2\left(\xi^2+\omega_2^2\right)}, \end{aligned} \tag{B1}$$

$$y(t) = -\frac{e^{-\xi t}}{\xi}C_{1y} + C_{2y} - F_1\frac{\xi\cos(\omega_1 t) + \omega_1\sin(\omega_1 t)}{\omega_1\left(\xi^2+\omega_1^2\right)} - F_2\frac{\xi\cos(\omega_2 t) + \omega_2\sin(\omega_2 t)}{\omega_2\left(\xi^2+\omega_2^2\right)}. \quad \text{(B2)}$$

The constants $C_{1x,y}$ and $C_{2x,y}$ are determined by the initial conditions of the system. The parameter ϕ is equal to zero for circular and inward flower patterns, and it is equal to π for the outward flower patterns.

The values of both angular frequencies ω_1 and ω_2 and forcing amplitudes F_1 and F_2 can be directly determined from the spiral tip pattern of the spatially extended models. First, the frequencies are found explicitly from the Fourier power spectrum of the coordinates for the tip trajectory, as shown in Fig. 2(a). Second, explicit expressions for the forcing amplitudes can be derived by determining the maximum value, A_1, and minimum value, A_2, of $r = x^2 + y^2$, the spatial extent of the tip trajectory [see Fig. 2(b)]. This results in the following expressions for the forcing amplitudes:

$$F_1 = \frac{1}{2}\omega_1(A_1 + A_2)\sqrt{\xi^2+\omega_1^2}, \quad \text{(B3)}$$

$$F_2 = \omega_2\sqrt{\xi^2+\omega_2^2}\left(A_1 - \frac{F_1}{\omega_1\sqrt{\xi^2+\omega_1^2}}\right). \quad \text{(B4)}$$

Resulting values for the SP model parameters are given in Table III.

Anisotropy can also be incorporated into the SP model. For simplicity we will only consider FK set I. For this case, the tip trajectory in the presence of anisotropy becomes an ellipse with a long/short axis given by A_{1x} and A_{1y}, respectively. The amplitude of the forcing term in the SP model for x is now given by

$$F_{1x} = \omega_1 A_{1x}\sqrt{\xi^2+\omega_1^2}, \quad \text{(B5)}$$

with a similar expression for the forcing amplitude in the y equation. Figure 8 shows that the SP model can accurately capture the tip dynamics of the anisotropic FK model.

[1] K. J. Lee, E. C. Cox, and R. E. Goldstein, Phys. Rev. Lett. **76**, 1174 (1996).
[2] N. Gorelova and J. Bureš, Dev. Neurobiol. **14**, 353 (1983).
[3] S. Jakubith, H. H. Rotermund, W. Engel, A. Von Oertzen, and G. Ertl, Phys. Rev. Lett. **65**, 3013 (1990).
[4] I. R. Epstein and K. Showalter, J. Phys. Chem. **100**, 13132 (1996).
[5] A. T. Winfree, Science **175**, 634 (1972).
[6] A. Karma, Annu. Rev. Condens. Matter Phys. **4**, 313 (2013).
[7] C. M. Gray, A. K. Engel, P. König, and W. Singer, Visual Neurosci. **8**, 337 (1992).
[8] R. Gray, A. Pertsov, and J. Jalife, Nature **392**, 75 (1998).
[9] S. M. Narayan, D. E. Krummen, K. Shivkumar, P. Clopton, W.-J. Rappel, and J. M. Miller, J. Am. Coll. Cardiol. **60**, 628 (2012).
[10] S. M. Narayan, D. E. Krummen, and W.-J. Rappel, J. Cardiovasc. Electrophysiol. **23**, 447 (2012).
[11] S. M. Narayan, D. E. Krummen, M. W. Enyeart, and W.-J. Rappel, PLoS ONE **7**, e46034 (2012).
[12] A. T. Winfree, Chaos: Interdisc. J. Nonlin. Sci. **1**, 303 (1991).
[13] H. Zhang and A. Holden, Chaos, Solitons Fractals **5**, 661 (1995).
[14] V. Biktashev and A. Holden, Physica-Sec. D **116**, 342 (1998).
[15] Z. Qu, J. N. Weiss, and A. Garfinkel, Phys. Rev. E **61**, 727 (2000).
[16] Z. Qu, F. Xie, A. Garfinkel, and J. N. Weiss, Ann. Biomed. Eng. **28**, 755 (2000).
[17] P. Ashwin, I. Melbourne, and M. Nicol, Physica D: Nonlin. Phenom. **156**, 364 (2001).
[18] F. H. Fenton, E. M. Cherry, H. M. Hastings, and S. J. Evans, Chaos **12**, 852 (2002).
[19] V. Zykov, A. Krekhov, and E. Bodenschatz, Proc. Natl. Acad. Sci. USA **114**, 1281 (2017).
[20] M. Fink, S. A. Niederer, E. M. Cherry, F. H. Fenton, J. T. Koivumäki, G. Seemann, R. Thul, H. Zhang, F. B. Sachse, D. Beard *et al.*, Prog. Biophys. Mol. Biol. **104**, 2 (2011).
[21] S. R. Kharche, I. V. Biktasheva, G. Seemann, H. Zhang, and V. N. Biktashev, BioMed Res. Int. **2015**, 731386 (2015).
[22] M. Haissaguerre, A. J. Shah, H. Cochet, M. Hocini, R. Dubois, I. Efimov, E. Vigmond, O. Bernus, and N. Trayanova, J. Physiol. **594**, 2387 (2016).
[23] W.-J. Rappel, J. A. B. Zaman, and S. M. Narayan, Circ.: Arrhyth. Electrophysiol. **8**, 1325 (2015).
[24] C. Antzelevitch, Heart Rhythm **4**, 964 (2007).
[25] R. S. Oakes, T. J. Badger, E. G. Kholmovski, N. Akoum, N. S. Burgon, E. N. Fish, J. J. Blauer, S. N. Rao, E. V. DiBella, N. M. Segerson *et al.*, Circulation **119**, 1758 (2009).
[26] M. Haissaguerre, M. Hocini, A. Denis, A. J. Shah, Y. Komatsu, S. Yamashita, M. Daly, S. Amraoui, S. Zellerhoff, M. Q. Picat, A. Quotb, L. Jesel, H. Lim, S. Ploux, P. Bordachar, G. Attuel, V. Meillet, P. Ritter, N. Derval, F. Sacher, O. Bernus, H. Cochet, P. Jais, and R. Dubois, Circulation **130**, 530 (2014).
[27] X. Zou, H. Levine, and D. A. Kessler, Phys. Rev. E **47**, R800(R) (1993).
[28] F. Xie, Z. Qu, and A. Garfinkel, Phys. Rev. E **58**, 6355 (1998).
[29] D. Olmos, Phys. Rev. E **81**, 041924 (2010).
[30] C. W. Zemlin and A. M. Pertsov, Phys. Rev. Lett. **109**, 038303 (2012).
[31] A. Defauw, P. Dawyndt, and A. V. Panfilov, Phys. Rev. E **88**, 062703 (2013).
[32] P. Bittihn, S. Berg, U. Parlitz, and S. Luther, Chaos: Interdisc. J. Nonlin. Sci. **27**, 093931 (2017).
[33] S. Alonso, M. Bär, and B. Echebarria, Rep. Prog. Phys. **79**, 096601 (2016).
[34] F. Fenton and A. Karma, Chaos **8**, 20 (1998).
[35] J. T. Koivumaki, T. Korhonen, and P. Tavi, PLoS Comput. Biol. **7**, e1001067 (2011).
[36] D. M. Lombardo, F. H. Fenton, S. M. Narayan, and W.-J. Rappel, PLoS Comput. Biol. **12**, e1005060 (2016).
[37] J. T. Koivumaki, G. Seemann, M. M. Maleckar, and P. Tavi, PLoS Comput. Biol. **10**, e1003620 (2014).

[38] M. Wilhelms, H. Hettmann, M. M. Maleckar, J. T. Koivumaki, O. Dossel, and G. Seemann, Front Physiol. **3**, 487 (2012).
[39] D. M. Lombardo and W.-J. Rappel, Chaos: Interdisc. J. Nonlin. Sci. **27**, 093914 (2017).
[40] A. Wolf, J. B. Swift, H. L. Swinney, and J. A. Vastano, Physica D: Nonlin. Phenom. **16**, 285 (1985).
[41] I. V. Biktasheva and V. N. Biktashev, Phys. Rev. E **67**, 026221 (2003).
[42] J. Langham and D. Barkley, Chaos: Interdisc. J. Nonlin. Sci. **23**, 013134 (2013).
[43] V. N. Biktashev, D. Barkley, and I. V. Biktasheva, Phys. Rev. Lett. **104**, 058302 (2010).
[44] I. V. Biktasheva, D. Barkley, V. N. Biktashev, and A. J. Foulkes, Phys. Rev. E **81**, 066202 (2010).
[45] D. Barkley, Phys. Rev. Lett. **72**, 164 (1994).
[46] B. Sandstede and A. Scheel, Phys. Rev. Lett. **86**, 171 (2001).
[47] L. Xu, Z. Li, Z. Qu, and Z. Di, Phys. Rev. E **85**, 046216 (2012).
[48] S. Weinberg, S. Iravanian, and L. Tung, Biophys. J. **95**, 1138 (2008).
[49] J. Jalife, O. Berenfeld, and M. Mansour, Cardiovasc. Res. **54**, 204 (2002).